Zoosymposia 15: 159–171 (2019)
http://www.mapress.com/j/zs/

ISSN 1178-9905 (print edition)
ZOOSYMPOSIA
ISSN 1178-9913 (online edition)

http://dx.doi.org/10.11646/zoosymposia.15.1.18
http://zoobank.org/urn:lsid:zoobank.org:pub:B2C26C48-826D-4EB6-8B15-45BE2A1FDBC4

A geometric morphometric analysis of *Arachnoides placenta* (Echinoidea: Clypeasteroida): An examination of ontogenetic development and morphological variation

ROBERT E. SWISHER[1, 2] & JIH-PAI LIN[1]

[1] *Department of Geosciences, National Taiwan University, Taiwan*
[2] *Sam Noble Museum of Natural History, University of Oklahoma, USA*
Corresponding author: Jih-Pai Lin: NTU Post Office (Branch No. 23), P.O. Box 097, Taipei City 10699, Taiwan, email: jplin@hotmail.com; xyloplax1@gmail.com, phone: +886-2-33662928

Abstract

Irregular echinoids, particularly clypeasteroids or "sand dollars", have obtained highly adaptive morphologies suited to their life habitats. Specimens (n = 26) of a clypeasteroid echinoid *Arachnoides placenta* were examined to understand how these adaptive morphologies were ontogenetically and developmentally obtained. Ontogenetically, early post-larval juvenile specimens have a pentagonal morphologic outline (known as ambitus) that shifts to a circular or a sub-circular morphology observed in the largest adult specimens. Circular morphology appears optimized for the adult life habitat or niche. Both landmark and semilandmark geometric morphometric methodologies were applied to quantify shape change, ontogenetic variation, and developmental morphology in *A. placenta*. Ambitus change is concentrated along the interambulacral regions with broader curvature variations occurring across both ambulacral and interambulacral regions. Circular adult morphology was a result of non-isometric shape change concentrated anteriorly with minor variation around posterior margin/periproctal furrow. Interior morphologic change of the petaloids and periproct was also quantified, mainly impacting posterior outline morphology. Minimal deformation of the basicoronal plates was detected, indicating stability during ontogeny. Results indicated that complex, non-isometric allometric shape change, both along the ambitus and interiorly, is required to morph from a pentagonal outline in post-larval juveniles to a circular or sub-circular ambitus morphology in adults. This analysis demonstrates the advantages of both landmark and semilandmark geometric morphometric analyses for quantifying developmental change and shape variation in Clypeasteroida.

Key words: sand dollars, ontogeny, geometric morphometrics, Clypeasterina, Taiwan

Introduction

Evolution of clypeasteroids is relatively young geologically. Clypeasteroida (Agassiz 1872) and members of the family Clypeasteridae (Agassiz 1835) are first recorded in the late Paleocene, continuing into the present (Kier 1982). Morphologically, clypeasteroids have obtained variable shapes ranging from elongate, strongly bilateral appearances, to nearly circular and sub-circular outlines, with morphology strongly optimized for life habitats (Durham 1955; Seilacher 1979). This study examines *Arachnoides placenta* (Linnaeus 1758) to better understand how a distinctive, near circular outline is obtained. *Arachnoides placenta* is one of the most common sand dollar in the Indo-West Pacific (McNamara *et al.* 2017; Schultz 2017; Lee *et al.* in press). Ontogenetically, post-larval juveniles become readily apparent at approximately 3mm in length in an open marine setting (Chen & Hsieh 1994). Strong allometric shape change during ontogeny is readily apparent for the *A. placenta* data set examined in this analysis (Fig. 1). Smallest post-larval juveniles appear to have an outline morphology less adaptive to the adult life-style habitat, with a strongly pentagonal outline (Figs. 1a,

Accepted by T. Oji: 7 Mar. 2019; published: 21 Oct. 2019

1c), while the largest adult samples of *A. placenta* obtain a distinctive circular outline while retaining remnants of bilateral symmetry (Figs. 1b, 1d). The pentagonal outline develops early in post-larval juveniles and is visible in specimen at approximately 5mm in length (Seilacher 1979). Previous studies on irregular echinoids support the hypothesis that clypeasteroids have more specialized morphologies adapted for high-energy, shallow intertidal settings (Brown 1983; Kanazawa 1992; Cabanac & Himmelman 1996; Saitoh & Kanazawa 2012). This study utilizes geometric morphometric analyses to assess ontogenetic development of circular morphology and developmental variation in clypeasteroid echinoids. While some holistic morphometric and geometric morphometric work has been conducted using echinoid data (Moore & Ellers 1993; Sievers & Nebelsick 2014; Zachos 2015; Schlüter 2016), this analysis focuses on developing, testing, and expanding the application of geometric morphometric methodologies for clypeasteroids exemplified by *A. placenta*. The goal of study is to examine how *A. placenta* obtained a circular to sub-circular ambitus during post-larval ontogeny.

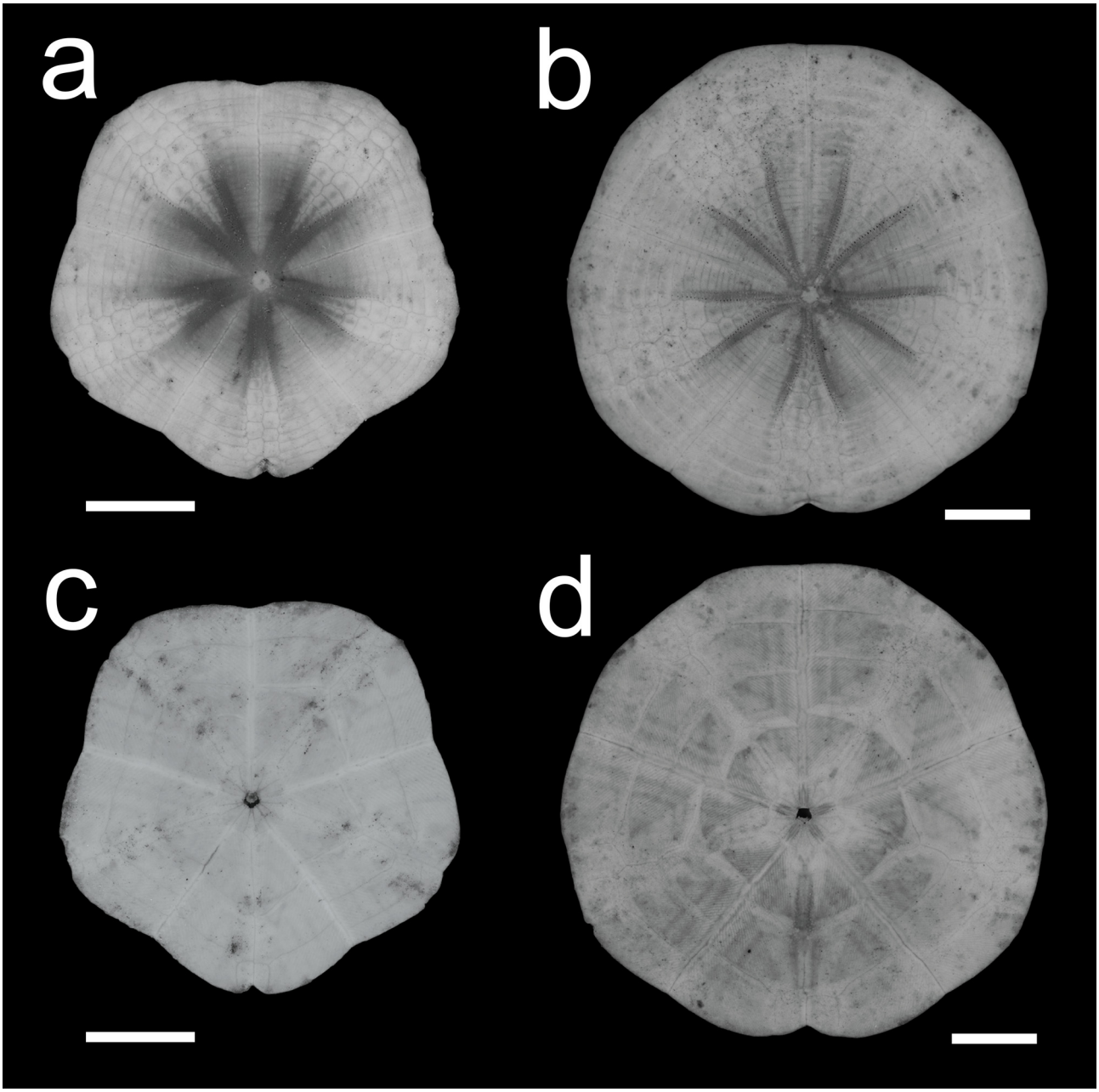

FIGURE 1. Ontogenetic morphological and outline shape variations between smaller juveniles and adult morphologies in *Arachnoides placenta*. A, C, Smaller juvenile *A. placenta* specimen (NTUG-SD-AP-105) exhibiting a stronger bilateral symmetry and a sub-pentagonal outline, aboral view in A, oral view in C. B,D, Large, adult *A. placenta* specimen (NTUG-SD-AP-101) exhibiting a circular/sub-circular outline, with reduced bilateral symmetry, aboral view in B, oral view in D. Scale bars = 1 cm.

Methods

Study samples

The analysis quantifies ambitus curvature, the distal edges of the basicoronal plates, and petaloid shape through digitization of landmark and semilandmark points based on the historical clypeasteroid collections housed at the Department of Geosciences, National University of Taiwan (NTUG). A total of 26 individuals (from NTUG-SD-AP-101 to NTUG-SD-AP-126) were examined, comprising an ontogenetic series from smaller juveniles to full adult morphotypes. Specimen range in size from approximately 3 cm to 5.5 cm in length. Standard morphologic terminologies follow the illustrated key in Mooi (1989). Analyses of developmental and ontogenetic shape variation in *Arachnoides placenta* were conducted using geometric morphometric methodologies outlined in Bookstein (1991), Zelditch *et al.* (2004), and Webster & Sheets (2010). Specimens were oriented for photography parallel to the bilateral plane of symmetry with periproct positioned posteriorly in both oral and aboral views (Fig. 2). Landmark and semilandmark data were digitized using TpsDig 2.31 software (Rohlf 2015; Rohlf 2018). Landmark data was collected in both oral and aboral views, while semilandmark data was only collected in aboral view because ambitus curvature is the same in both aboral and oral views. Among 26 specimens, four specimens (NTUG-SD-AP-109, NTUG-SD-AP-110, NTUG-SD-AP-113, and NTUG-SD-AP-121) were excluded from the analysis due to test damage or developmental abnormalities. A total of 20 specimens was included for the oral view landmark analysis (NTUD-SD-AP-108 and NTUD-SD-AP-122 excluded); 22 specimens were used for the aboral view landmark analysis; and 20 specimens were used for the semilandmark analysis (NTUD-SD-AP-103, NTUD-SD-AP-122 excluded). Landmark points were chosen to maximize observable variation within and between growth plates while providing an optimal summary of ambitus curvature, the distal edges of basicoronal plates, and petaloid shape. Landmark data was digitized on both sides of the axial plane as mirrored pairs. Paired landmark data was averaged following methodologies outline in Zelditch *et al.* (2004) and Zelditch (2005) since they cannot be regarded as independent. Because this is an analysis of shape and curvature variation only, and not an analysis of asymmetry within the data set including information on both the left and rights of approximately bilaterally symmetrical specimen would be redundant for the presented geometric morphometric analysis (Zelditch *et al.* 2004). Asymmetry within sand dollars during ontogeny has previously been reported (Collin 1997); future studies will attempt to quantify asymmetry between data sets, species, and clypeasteroid groups, but at this time is beyond the scope of the current analysis. Digitized landmark and semilandmark points for the aboral and oral views are illustrated (Figs. 2a–2c). Principle components analyses (PCA) were performed to observe and quantify shape variation in the *A. placenta* data was and through subsequent visual comparison of produced thin-plate warp spline deformation grids (Figs. 3–5). Because this was an initial study with the goal of developing methodologies for landmark and semilandmark analysis for both extant and fossil clypeasteroid irregular echinoid data sets, only observable ontogenetic growth change and developmental variation in the *A. placenta* was examined currently. Collected landmark and semilandmark data were analyzed using Integrated Morphometrics Package (IMP) software CoordGen8 and PCAGen8 (Sheets 2001; Zelditch *et al.* 2004; Zelditch *et al.* 2012).

Previous work (Schlüter 2016) has applied geometric morphometric methodologies to examine fluctuating asymmetry and ecophenotypic variation in the spatangoid *Micraster (Gibbaster) brevis*. As this analysis of *Arachnoides placenta* only examines one collection we are unable to assess at this time to what degrees, if any, fluctuating asymmetry and ecophenotypic variation exists between and effects the morphology of *Arachnoides* populations; this however does present an intriguing opportunity for future comparative research.

Landmark analysis of oral surface

A total of 26 landmarks were digitized in oral view (Fig. 2a): 4 landmarks along the axis (points 1, 11, 12, and 24 in Fig. 2a); 9 paired ambitus landmarks on opposite sides of the axis (points 2–10 and 13–21 in Fig. 2a); and 2 paired interior landmarks on opposite sides of the axis placed at the tips of the basicoronal plates (points 22, 23, 25, 26 in Fig. 2a). Point 1 is at the junction of the perradial suture with ambitus in ambulacral region III. Point 11 is at the junction of the interradial suture with ambitus in interambulacral region 5. Point 12 is placed at posterior end of peristome. Point 24 is placed at the posterior end of the basicoronal plate. Points 2, 4, 6, 8, 10 are placed at the junction of the adradial sutures with ambitus. Points 3 and 7 are placed at the junction of the interradial sutures with ambitus. Points 5 and 9 are placed at the junction of the perradial sutures with ambitus. Points 22 and 23 are placed at the distal tips of basicoronal plates. Mirrored points are

shaded in Figure 2a. Among the 26 points, 22 paired landmarks were averaged along the axis and plotted on the left side of the test, resulting in a total of 15 landmark points illustrated in analyses (Fig. 3).

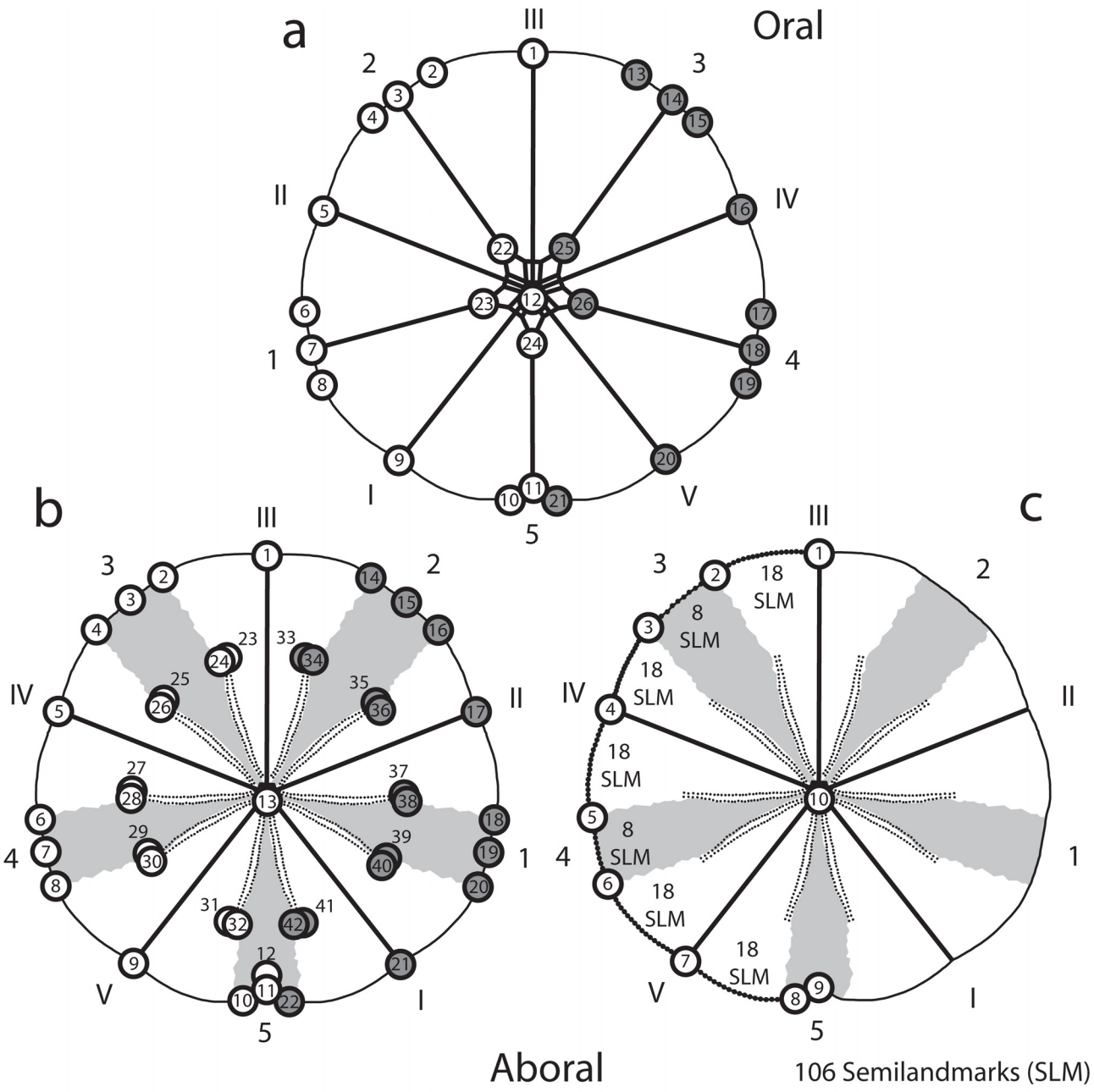

FIGURE 2. Landmark and semilandmark configuration for geometric morphometric analysis of *Arachnoides placenta* data. Landmarks are indicated by numbers in circles. A, Landmark data points for *A. placenta*, oral view. Landmarks 1–11 and paired homologous landmarks 13–21, grey circles, are analogous to those described in aboral view (see Fig. 2b); 12, midpoint taken at the posterior end of peristome along the axis; 22–24, basicoronal plates surrounding the peristome, taken at the distal tips of basicoronal plates. 25–26, grey circles, are paired with homologous landmarks to 22–23, white circles. B, Landmark data points for *A. placenta*, aboral view. 1, Anterior most perradial suture in the ambulacral region (III); 2, 4, 6, 8, 10, adradial sutures; 3, 7, interradial sutures; 5, 9 perradial sutures; 11, posterior margin of interradial suture in the interambularal region (5); 12, periproct, taken at the posterior periproct margin along the axis; 13, midpoint taken at the posterior end of the apical disc along the axis at the junction with the interradial suture; 14–22, grey circles, are paired with homologous landmarks 2–10 (indicated by white circles); 23–32, paired landmarks indicating the distal pore pairs in the petaloids; 33–42, grey circles, are paired with homologous landmarks 23–32 (indicated by white circles). C, Semilandmark data points, bounded by landmark data points for *A. placenta*, aboral view. 1, Anterior most perradial suture in the ambulacral region (III); 2, 3, 5, 6, 8, adradial sutures; 4, 7, perradial sutures; 9, posterior notch in the interambulacral region (5); 10, midpoint taken at the posterior end of the apical disc along the axis. Semilandmarks are indicated by smaller, unnumbered circles that summarize the curvature from the anterior midpoint to the posterior midpoint, left side.

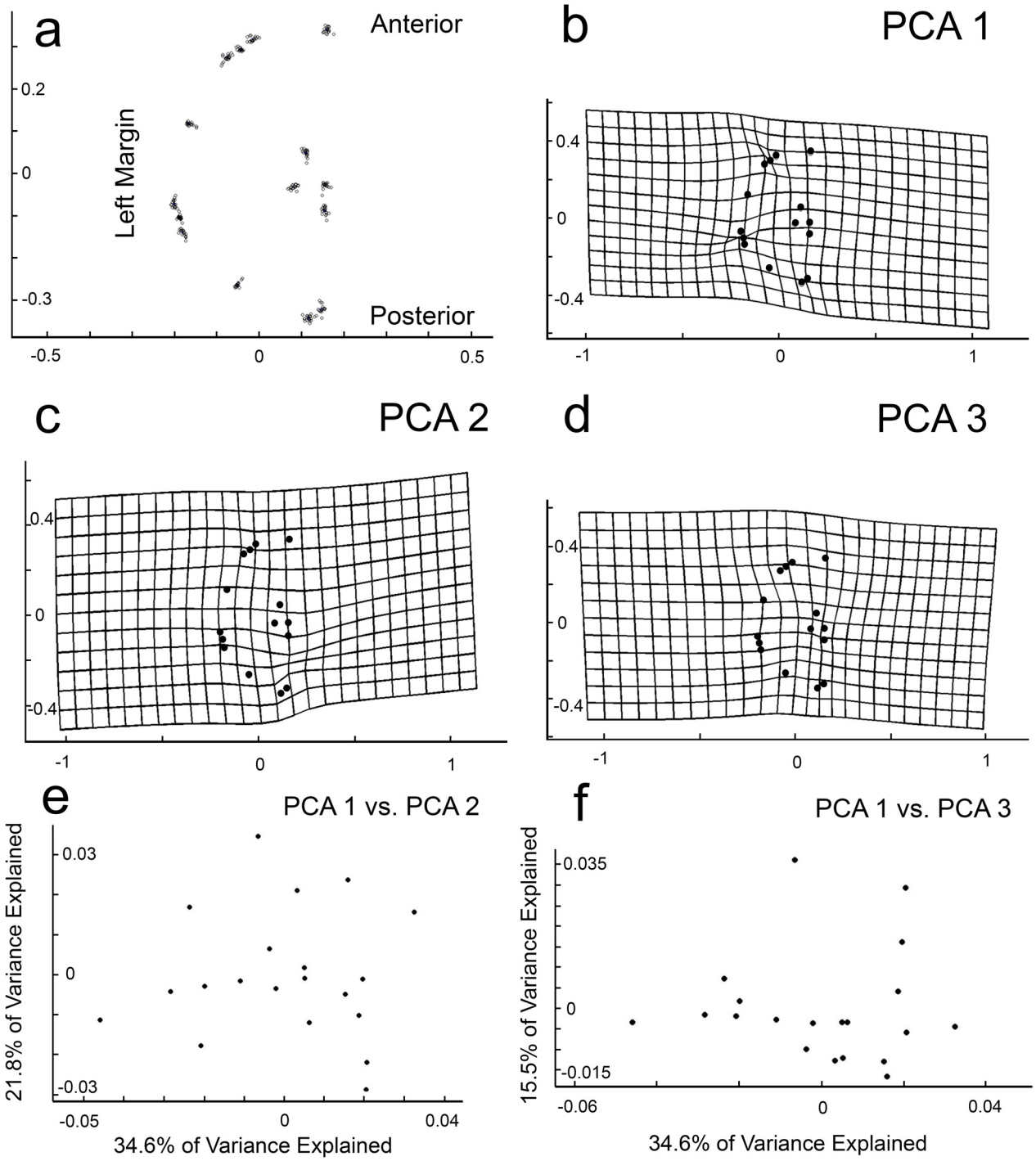

FIGURE 3. Warp-spline deformation grids (Procrustes) and PCA plots from the PCA (principle components analysis) for the landmark data of *Arachnoides placenta*, oral view. PCA 1, PCA 2, and PCA 3 presented are accounting for 71.9% of observed morphological variance within the data set. Landmark configuration is presented in Figure 2a. A, Landmark data plot for *A. placenta* specimens (Procrustes). B, Warp-spline deformation grid for PCA 1, 34.6% of total variance explained. C, Warp-spline deformation grid for PCA 2, 21.8% of total variance explained. D, Warp-spline deformation grid for PCA 3, 15.5% of total variance explained. Scaling factor 0.1 for all deformation grids (Procrustes). E, PCA plot for PCA 1 (x-axis) vs PCA 2 (y-axis). F, PCA plot for PCA 1 (x-axis) vs PCA 3 (y-axis).

Landmark analysis of aboral surface

A total of 42 landmarks were digitized in aboral view (Fig. 2b): 4 landmarks along the axis (points 1, 11, 12, and 13 in Fig. 2b); 9 paired ambitus landmarks on opposite sides of the axis (points 2–10 and 14–22 in Fig.

2b); and 10 paired interior landmarks on opposite sides of the axis placed at the distal most podial pore pairs of the petaloids (points 23–32, and 33–42 in Fig. 2b). Point 1 is at the junction of the perradial suture with ambitus in ambulacral region III. Point 11 is at the junction of the interradial suture with ambitus in interambulacral region 5. Point 12 is placed at the posterior periproct margin with the interradial suture. Point 13 is placed at the posterior margin of the apical disc. Points 2, 4, 6, 8, 10 are placed at the junction of the adradial sutures with ambitus. Points 3 and 7 are placed at the junction of the interradial sutures with ambitus. Points 5 and 9 are placed at the junction of the perradial sutures with ambitus. Points 23–32 are placed at the distal positions of the petaloids based on the last distinguishable podial pore pairs. Previous quantitative work supports that the petaloid structures of *A. placenta* and other clypeasteroids maintain bilateral symmetry, suggesting petaloid structures are suitable features and points for landmark analysis (Lawrence *et al.* 1998). Mirrored points are shaded in Figure 2b. Among the 42 points, 38 paired landmarks were averaged along the axis and plotted on the left side of the test, resulting in a total of 23 landmark points illustrated in analyses (Fig. 3).

Semilandmark analysis of aboral surface

A total of 10 landmarks were digitized in aboral view (Fig. 2c), utilizing the ambitus landmark configuration described in the aboral view landmark analysis (Fig. 2b). For the analysis landmark points at the interradial sutures (Points 4 and 7, Fig. 2b) were excluded to maximize curvature data captured by digitized semilandmark points. A total of 106 semilandmarks were digitized, along seven marginal ambulacral and interambulacral curves (Fig. 2c). All semilandmark data are bounded by landmark data points (Fig. 2c). The semilandmark analysis was based on data collected from the left side of the specimen for comparison with landmark analyses.

For the semilandmarks analysis 18 points between landmarks 1–2 (Fig. 2c) were taken for summarizing the ambitus curvature in the ambulacral region (III). 8 points between landmarks 2–3 (Fig. 2c) were taken for summarizing ambitus curvature in the interambulacral area (3). 18 points between landmarks 3–4 (Fig. 2c) were taken for summarizing ambitus curvature in the anterior portion of the ambulacral region (IV). 18 points between landmarks 4–5 (Fig. 2c) were taken for summarizing ambitus curvature in the posterior portion of the ambulacral region (IV). 8 points between landmarks 5–6 (Fig. 2c) were taken for summarizing lateral ambitus curvature in the interambulacral area (4). 18 points between landmarks 6–7 (Fig. 2c) were taken for summarizing posterior-lateral ambitus curvature in the ambulacral region (V). 18 points between landmarks 7–8 (Fig. 2c) were taken for summarizing posterior ambitus curvature in the ambulacral region (V).

Shape variation in the *A. placenta* data set is quantified and visually compared through principal component analysis (PCA) and generated thin-plate spline deformation grids (Rohlf 1990; Bookstein 1991; Zelditch *et al.* 2004). As this analysis focused on developing methodologies for landmark and semilandmark analysis for *Arachnoides*, only observable ontogenetic growth change and developmental variation between species was tested at this time. Tests for asymmetry between specimens was not studied because it was beyond the scope of the analysis.

Results

Morphological shape variations within the observed ontogenetic series of *Arachnoides placenta* for the landmark analyses in oral and aboral views, and the semilandmark analysis in aboral view are summarized in Table 1 and present in Figures 3–5 respectively.

Broadly, ontogenetic morphology change is most strongly observed through shape and ambitus change from a juvenile pentagonal outline to an adult circular outline with remnants of bilateral symmetry. Geometric morphometric analyses of *A. placenta* indicate that growth patterns are not isometric, with shape change concentrated anteriorly and to some extent laterally. During ontogeny deformation occurs at the interambulacral regions at both the junctions with the adradial sutures and the interradial sutures with the ambitus, accompanied by reciprocal deformation in the ambulacral regions of the ambitus, leading to the shift from a pentagonal outline in smaller juveniles, to a more circular morphology in adult specimen. Rounding of the outline is concentrated anteriorly, with interambulacral deformation more strongly developed anteriorly. Outline morphology shifts during ontogeny are further supplemented by curvature change along the ambitus of the enlarging ambulacral regions, again concentrated more strongly anteriorly. Deformation of the adradial

and interradial sutures, accompanied by curvature change within the ambulacral regions appears to happen relatively late during ontogeny as only the largest specimens exhibit a distinctive circular outline. Internal shape variation of the petaloid structures and periproct suggests internal outward plate expansion occurred throughout ontogeny, however these growth patterns appear to have minimal effects on adult outline morphology and ambitus curvature. Minimal deformation is observed at the basicoronal plates.

TABLE 1. Summary of PCA and warp-spline deformation grids for the landmark analyses of the oral and aboral surfaces and the semilandmark analysis of the aboral surface.

	PCA 1	PCA 2	PCA 3	Sum
Landmark analysis of oral surface (Fig. 3)	34.6%	21.8%	15.5%	71.9%
Landmark analysis of aboral surface (Fig. 4)	43.8%	22.8%	8.7%	75.3%
Semilandmark analysis of aboral surface (Fig. 5)	44.8%	26.7%	9.1%	80.6%

Discussion

Landmark analysis of oral surface

PCA 1 relates to ambitus curvature change and deformation in the *A. placenta* data set (Fig. 3b). Deformation is concentrated at the interradial sutures and adradial sutures of the interambulacral regions. Though less pronounced and more uniformly dispersed, deformation is also noted along the ambitus margins of the ambulacral regions, occurring in junction with deformation at the adradial sutures and interradial sutures. PCA 2 is largely related to posterior deformation along the axis, posterior to the basicoronal plates, but anterior and internally to the posterior margin (Fig 3c). Minor interior deformation around the peristome and adjoining plates is noted. Subtle deformation occurred along the ambitus, again more highly concentrated within the interambulacral regions at the adradial sutures. PCA 3 is related to ambitus deformation, minor deformation at the basicoronal plates, and shape change within the ambulacral regions (Fig 3d). Deformation is concentrated within the ambitus and at the perradial sutures. Deformation occurs also within the basicoronal plates, but is relatively minor compared to deformation at along the ambitus.

PCA of Landmark analysis of oral surface

When PCA 1 vs. PCA 2 are plotted for the data set PCA 1 shows a progression from larger specimens (left) to smaller specimens (right) (Fig. 3e). Similarly, PCA 2 shows a grouping of larger specimens (bottom) to smaller specimen (top) (Fig. 3e). For both PCA 1 and PCA 2 larger specimens clustering more closely together while medium and smaller specimen show a much wider spread in distribution; particularly with PCA 2 (Fig. 3e).

The plot of PCA 1 vs. PCA 3 demonstrates a similar trend of larger specimens clustering more closely together while medium and smaller specimens show a wider spread in distribution, though with reduced spread compared to the PCA 1 vs. PCA 2 plot. PCA 3 has a much weaker control on specimen distribution, with only a few smaller specimens strongly controlled by PCA 3 (Fig. 3f).

Landmark analysis of aboral surface

PCA 1 relates almost exclusively to petaloid deformation in the *A. placenta* data set (Fig. 4b). Deformation is largely controlled by shape change and outward expansion within the petaloid structures, specifically at the outer-most podial pores and surrounding plates. PCA 2 relates to ambitus shape change and internal deformation (Fig. 4c). Ambitus deformation is concentrated along the adradial and perradial sutures. Internal deformation occurs in conjunction to observed ambitus deformation for both the ambulacral and interambulacral regions; however, deformation is only readily apparent near the ambitus, with deformation becoming increasingly diminished interiorly towards the apical disc. Minor interior deformation is also noted around the periproct. PCA 3 relates to posterior deformation along the axis (Fig. 4d). Deformation is

concentrated along the posterior margin and surrounding the periproct. Minor ambitus deformation is concentrated within the interambulacral margin and to a degree within the ambulacral margin, again concentrated at the perradial suture.

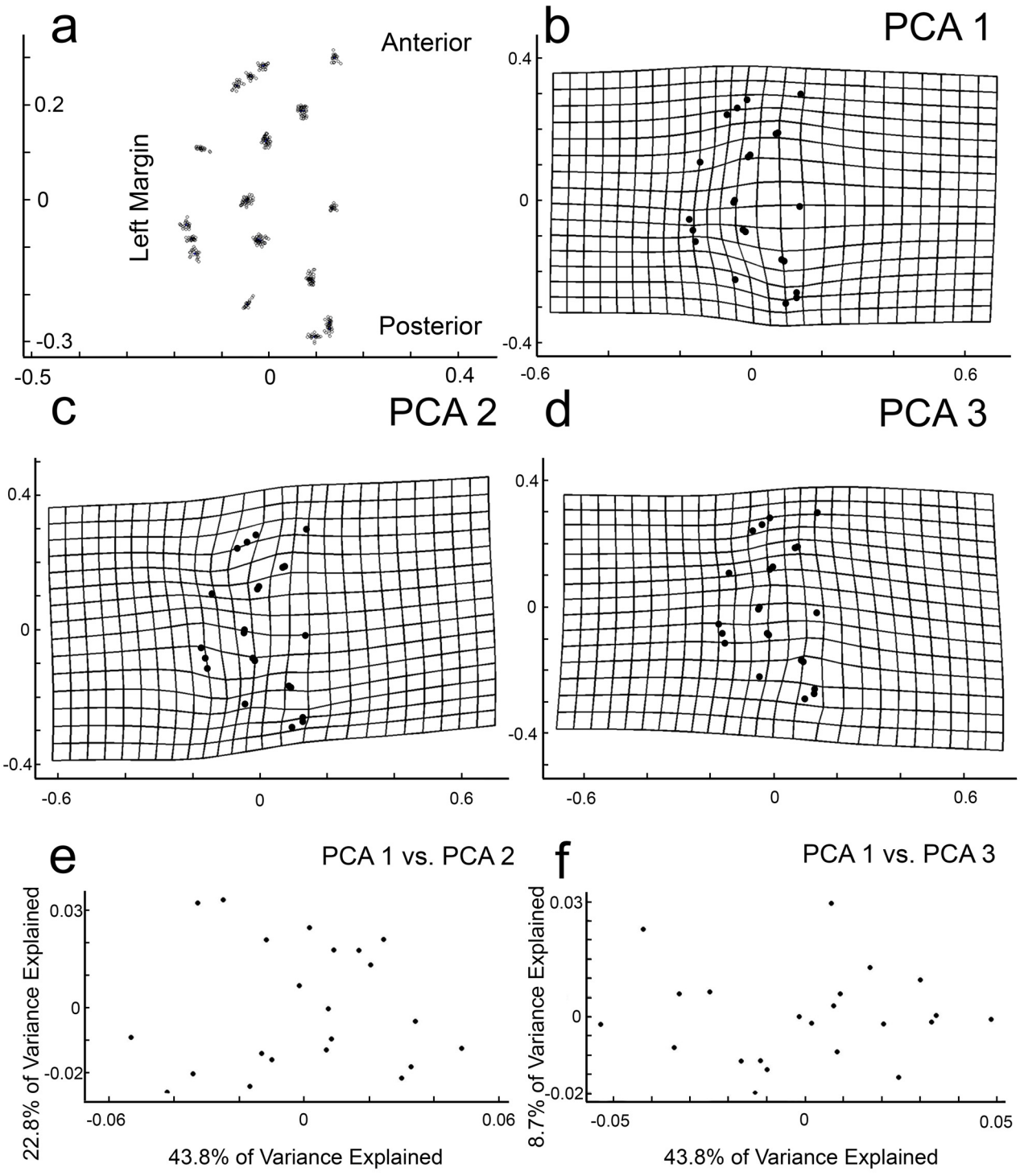

FIGURE 4. Warp-spline deformation grids (Procrustes) and PCA plots from the PCA (principle components analysis) for the landmark data of *Arachnoides placenta*, aboral view. PCA 1, PCA 2, and PCA 3 presented are accounting for 75.3% of observed morphological variance within the data set. Landmark configuration is presented in Figure 2b. A, Landmark data plot for *A. placenta* specimens (Procrustes). B, Warp-spline deformation grid for PCA 1, 43.8% of total variance explained. C, Warp-spline deformation grid for PCA 2, 22.8% of total variance explained. D, Warp-spline deformation grid for PCA 3, 8.7% of total variance explained. Scaling factor 0.1 for all deformation grids (Procrustes). E, PCA plot for PCA 1 (x-axis) vs PCA 2 (y-axis). F, PCA plot for PCA 1 (x-axis) vs PCA 3 (y-axis).

While there is some internal elevation in the aboral view centered around the apical disc and petaloid structures, overall the tests in *A. placenta* are relatively flat. As such, internal landmarks only capture shape variation along the aboral plane, and not related to internal elevation. No notable distortion appears across internal landmark data during ontological development for *A. placenta* that appears readily attributable to aboral elevation shifts, suggesting internal elevation has minimal effect on petaloid structural variation compared to shape variation along the aboral plane, at least for the landmark data used in this study. A more comprehensive analysis including internal or complete digitization of all podial pores into landmark data would likely capture position variation due to elevation during ontogeny, if present.

PCA of Landmark analysis of aboral surface

For the plot of PCA 1 vs. PCA 2, larger and medium sized specimens cluster in the upper portions of the plot, while smaller specimen are spread across the base of the plot, clustering more towards the bottom left (Fig. 4e). PCA 1 broadly divides the smaller and larger specimens to the left of the plot, with the medium specimens grouping more towards the right. PCA 1 seems to largely describe variation in petaloid morphology and this apparent grouping appears to support non-isometric growth over a linear growth pattern based on body size (Fig. 4e). PCA 2 appears to have the larger control on distribution based on specimen size (Fig. 4e). The plot of PCA 1 vs. PCA 2 likely has more complexity due to inclusion both of internal structures along with ambitus data.

In the plot of PCA 1 vs. PCA 3 a broad distribution in data is noted with no readily apparent groupings (Fig. 4f). This suggests PCA 3 is more randomized and may relate to non-isometric change within the data set.

Semilandmark analysis of aboral surface

PCA 1 almost exclusively relates to ambitus deformation (Fig. 5b). Deformation is concentrated along the anterior margin, with strongest deformation occurring within the anterior most interambulacral region beginning at the anterior most adradial suture (3 in Fig. 2c), posteriorly adjacent ambulacral margin (IV in Fig. 2c), and the second interambulacral region ending at the adradial suture (4 in Fig. 2c). Ambitus deformation also occurs along the posterior most ambulacral region (V in Fig. 2c) and posterior interambulacral region (5 in Fig. 2c), but deformation is subtle and relatively minor compared to observed anterior deformation. Strong anterior deformation is also noted at the anterior margin along the axis and posteriorly approaching the posterior margin and periproct. Posterior deformation might relate to movement of the periproct and the plates surrounding. PCA 2 relates to anterior ambitus deformation (Fig. 5c). Deformation is strongly concentrated along the anterior most interambulacral margin (3 in Fig. 2c) and within the anterior-most ambulacral margin (IV in Fig. 2c) immediately posterior to the interambulacral region (3 in Fig. 2c). Minor deformation occurs at the posterior margin along the axis, while all other margin and interior deformations are subtle and minor. PCA 3 largely relates to anterior deformation focused along the axis (Fig. 5d). Deformation is strongest along the ambitus (5 in Fig. 2c) and interiorly near the perradial suture (III in Fig. 2c) along the axis. Strong deformation is also noted along the margin and interiorly within the first interambulacral region, concentrated at the adradial sutures (3 in Fig. 2c) and to a lesser extent within the ambulacral region posteriorly adjacent to it (IV in Fig. 2c). Minor marginal deformation is noted laterally and posteriorly (regions 4 and V in Fig. 2c) but is relatively poorly defined.

PCA of Semilandmark analysis of aboral surface

The plot of PCA 1 vs. PCA 2 illustrates strong clustering of larger body size and circular ambitus curvature morphology (right side) and smaller body size and pentagonal ambitus morphology (left side) with gradation of mid-sized and intermediate morphologies in-between these two ends along the PCA 1 axis (Fig. 5e). PCA 2 tends to group smaller (upper left) and larger specimen (upper right) around the top of the plot. This suggests ambitus variation described by this PCA is strongly non-isometric during development (Fig. 5e).

The plot of PCA 1 vs. PCA 3 is strongly dominated by PCA 1 and the morphology/body size patterns described above for the plot of PCA 1 vs. PCA 2 (Fig. 5f). PCA 3 appears to show some trending of smaller and larger morphologies occurring closer the base of the plot, but distinct clustering or groupings are not readily apparent for PCA 3 (Fig. 5f).

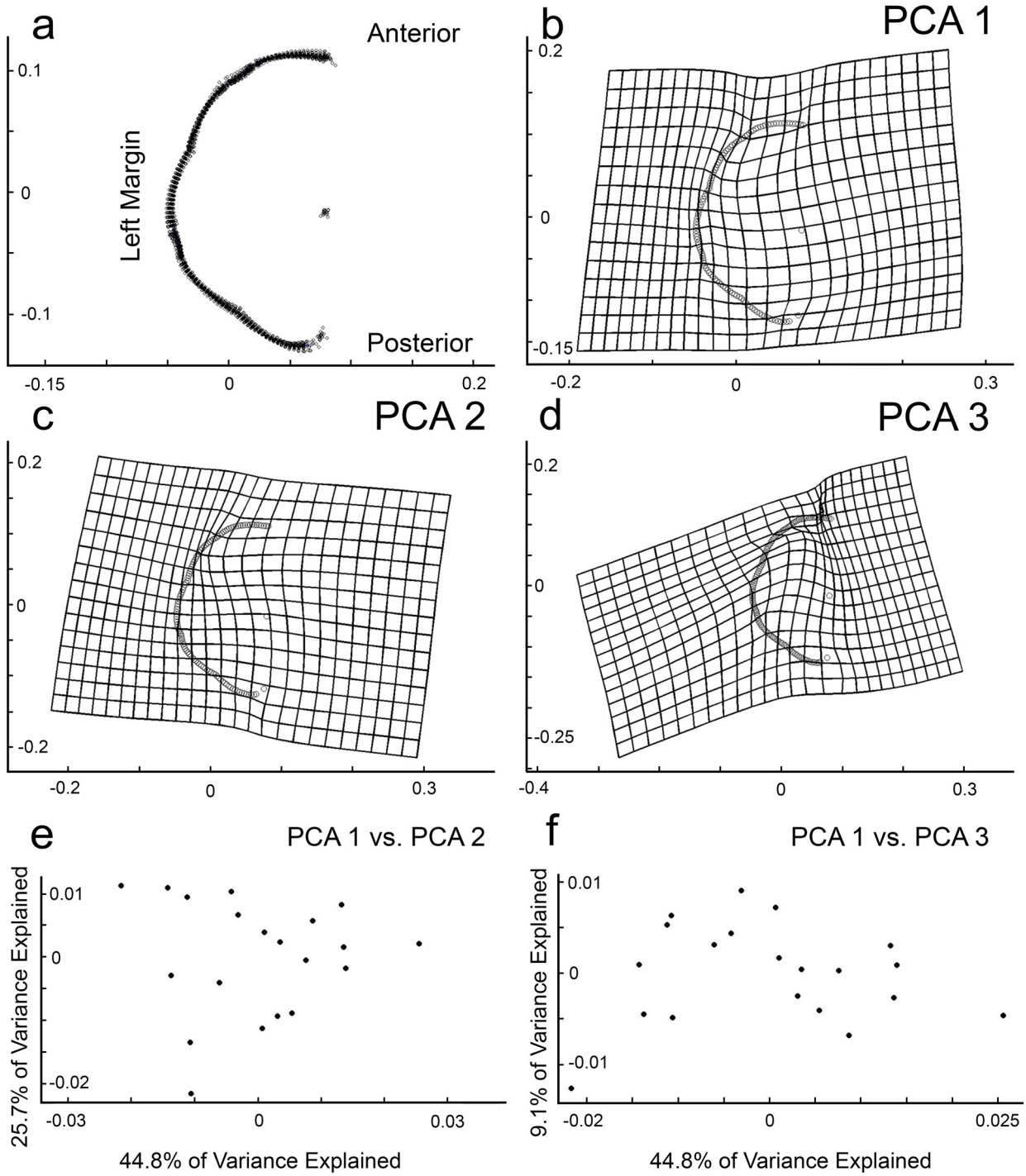

FIGURE 5. Warp-spline deformation grids (Procrustes) and PCA plots from the PCA (principle components analysis) for the semilandmark data of *Arachnoides placenta*, aboral view. PCA 1, PCA 2, and PCA 3 presented are accounting for 80.6% of observed morphological variance within the data set. Landmark and semilandmark configuration presented in Figure 2c. A, Semilandmark data plot for *A. placenta* specimens (Procrustes). B, Warp-spline deformation grid for PCA 1, 44.8% of total variance explained. C, Warp-spline deformation grid for PCA 2, 26.7% of total variance explained. D, Warp-spline deformation grid for PCA 3, 9.1% of total variance explained. Scaling factor 0.05 for all deformation grids (Procrustes). E, PCA plot for PCA 1 (x-axis) vs PCA 2 (y-axis). F, PCA plot for PCA 1 (x-axis) vs PCA 3 (y-axis).

In summary, these results suggest that a complex series of allometric growth patterns, shape, and curvature changes are required to shift from the pentagonal smaller juvenile to the observed circular adult morphology in *A. placenta*. This study also demonstrates the benefits of using multi-faceted approaches to

analyze morphological and developmental change in members of Clypeasteroida (sand-dollars). Landmark analyses of the oral and aboral surfaces identify loci of morphological and developmental change along the ambitus and internally accurately, with areas of deformation clearly identifiable. However, using landmark data alone, only limited interpretations can be made on ambitus curvature change during ontogeny due to missing data points within regions of large shape variation, the ambitus curvatures of the interambulacral and ambulacral areas. The semilandmark analysis provides a means to more accurately describe curvature variation across the ambitus as a whole and provides a detailed depiction of where morphological deformation is concentrated in the *A. placenta* dataset. These results suggest semilandmark analyses may be preferred for understanding ambitus variation as well as morphological variation of body shapes within Clypeasteroida, while landmark analyses provide a more accurate depiction of loci of morphological and developmental variation.

Conclusions

The study formed the basis for developing a methodology to assess ontogenetic, developmental, and morphological variation through geomorphic morphometric analysis for *Arachnoides* and other clypeasteroid echinoids. Oral surface landmark data of the warp-spline deformation grids demonstrated that adult *A. placenta* specimens have increased curvature indention and deformation concentrated at the interambulacral areas compared to pentagonal smaller juveniles (Fig. 3). Deformation was concentrated mainly around the interradial and adradial sutures during growth with corresponding deformation occurring along the ambulacral regions. A combined effect with observable deformation and ambitus change along and within the ambulacral regions and perradial sutures resulted in the observed circular/sub-circular adult morphology of *A. placenta*. This interpretation was further supported by the data obtained from the aboral surface (Fig. 4). Internal deformation based on petaloid and periproct landmark data suggests internal, centralized outward plate deformation was present during ontogeny but had minimal effects on overall ambitus curvature and shape change. However, internal morphologic plate shifts had a stronger effect posteriorly overall. Similarly, on the oral surface, deformation of the basicoronal plates is minimal, suggesting little change during ontogenetic development (Fig. 3).

Semilandmark analysis of the ambitus (Fig. 5) presented a more complex deformation pattern through the warp-spline deformation grid plots suggesting a similarly complex ontogenetic and developmental history for the *A. placenta* when compared with the landmark data. Observed deformation patterns for the oral and aboral surfaces through the ontogenetic series of *A. placenta* indicate the following trends. 1) Outline shape change is strongly concentrated within interambulacral regions at the adradial and interradial sutures (Figs. 3–5). Deformation within the interambulacral regions, particularly along the anterior ambitus, reshapes the pentagonal juvenile morphology into the circular/sub-circular adult morphology. 2) Ambitus outline is controlled by a combination of shifts, contractions, and variation in curvature within both the ambulacral and interambulacral regions. 3) Changes in curvature and outline are concentrated anteriorly (Fig. 5).

Acknowledgements

This manuscript cannot be completed without the constructive comments provided by the guest editor Tatsuo Oji and two reviewers Tobias Grun and Andrea Kroh. This study was funded by Ministry of Science and Technology, Taiwan, ROC (MOST 107-2811-M-002-3125 and MOST 108-2811-M-002-608 to RES; and MOST 106-2116-M-002-018, MOST 107-2116-M-002-007 and MOST 108-2116-M-002-014 to JPL).

References

Agassiz, A. (1872–1874) *Revision of the Echini*. Illustrated Catalogue of the Museum of Comparative Zoölogy at Harvard College, 7, pt. 1–2: i–xii, 1–378, pls. 1–49 (1872), pt. 3, 379–628+1, pls. 50–77, (1873), pt. 4, 629–762, pls. 78–94, (1874).

Agassiz, L. (1835) Prodrome d'une monographie des Radiaires ou Échinodermes. *Mémoires de la Société des Sciences Naturelles de Neuchâtel*, 1, 168–199.

Bookstein, F.L. (1991) *Morphometric Tools for Landmark Data: Geometry and Biology*. Cambridge University Press, Cambridge, 435 pp.
https://doi.org/10.1017/CBO9780511573064

Brown, C.L. (1983) Substrate preference and test morphology of a sand dollar (*Echinarachnius parma*) population in the Gulf of Maine. *Bios*, 54, 246–254.

Cabanac, A. & Himmelman, J.H. (1996) Population structure of the sand dollar *Echinarachnius parma* in the subtidal zone of the northern Gulf of St. Lawrence, eastern Canada. *Canadian Journal of Zoology*, 74, 698–709.
https://doi.org/10.1139/z96-079

Chen, C.P. & Hsieh, H.L. (1994) *A Basic Guide to Farm Marine Invertebrates*. National Museum of Marine Biology & Aquarium, Pingdong. [In Chinese]

Collin, R. (1997) Ontogeny of subtle skeletal asymmetries in individual larvae of the sand dollar *Dendraster excentricus*. *Evolution*, 51 (3), 999–1005.
https://doi.org/10.2307/2411175

Durham, J.W. (1955) Classification of clypeasteroid echinoids. *University of California Publications in Geological Sciences*, 31, 73–198.

Kanazawa, K. (1992) Adaptation of test shape for burrowing and locomotion in spatangoid echinoids. *Palaeontology*, 35, 733–750.

Kier, P. (1982) Rapid Evolution in Echinoids. *Paleontology*, 9, Part 1, 1–9, pls. 1–2.

Lawrence, J.M., Pomory, C.M., Sonnenholzner, J. & Chao, C.-M. (1998) Bilateral symmetry of the petals in *Mellita tenuis*, *Encope micropora*, and *Arachnoides placenta* (Echinodermata: Clypeasteroida. *Invertebrate Biology*, 117, 94–100.
https://doi.org/10.2307/3226855

Lee, H., Lin, J.P., Li, H.C., Chang, L.Y., Lee, K.S., Lee, S.J., Chen, W.J., Sankar, A. & Kang, S.C. (in press) Young colonization history of a widespread sand dollar (Echinodermata; Clypeasteroida) in western Taiwan. *Quaternary International*. [in Press]
https://doi.org/10.1016/j.quaint.2018.12.003

Linnaeus, C. (1758) Systema *Naturae per regna tria naturae, secundum classes, ordines, genera, species, cum characteribus, differentiis, synonymis, locis*, ii. Editio decima, reformata, Laurentius Salvius, Holmiae, 824 pp.
https://doi.org/10.5962/bhl.title.542

McNamara, K.J., Pawson, D.L., Miskelly, A.D. & Byrne, M. (2017) Class Echinoidea. *In:* Byrne, M. & O'Hara, T.D. (Eds.), *Australian Echinoderms: Biology, Ecology and Evolution*. CSIRO Publishing, Clayton South, pp. 351–445.

Mooi, R. (1989) Living and fossil genera of the Clypeasteroida (Echinoidea: Echinodermata): An illustrated key and annotated checklist. *Smithsonian Contributions to Zoology*, 488, 1–60.
https://doi.org/10.5479/si.00810282.488

Moore, A.M.F. & Ellers, O. (1993) A functional morphospace, based on dimensionless numbers, for a circumferential, calcite, stabilizing structure in sand dollars. *Journal of Theoretical Biology*, 162, 253–266.
https://doi.org/10.1006/jtbi.1993.1086

Rohlf, F.J. (1990) Rotational fit (Procrustes) methods. *In:* Rohlf, F.J. & Bookstein F.L. (Eds.), *Proceedings of the Michigan Morphometrics Workshop*, 2. University of Michigan, Special Publication, pp. 227–236.

Rohlf, F.J. (2015) The tps series of software. *Hystrix, the Italian Journal of Mammalogy*, 26, 1–4.

Rohlf, F.J. (2018) tpsDig, digitize landmarks and outlines, version 2.31. Department of Ecology and Evolution, State University of New York at Stony Brook.

Saitoh, M. & Kanazawa, K. (2012) Adaptive morphology for living in shallow water environments in spatangoid echinoids. *Zoosymposia*, 7, 255–265.
http://dx.doi.org/10.11646/zoosymposia.7.1.24

Schlüter, N. (2016) Ecophenotypic Variation and Developmental Instability in the Late Cretaceous Echinoid *Micraster brevis* (Irregularia; Spatangoida). *PLoS ONE*, 11 (2), 1–26.
https://doi.org/10.1371/journal.pone.0148341

Schultz, H. (2017) *Echinoidea, Volume 2: Echinoidea with Bilateral Symmetry. Irregularia*. Walter de Gruyter GmbH, Berlin, 359 pp.
https://doi.org/10.1515/9783110368536

Seilacher, A. (1979) Constructional morphology of sand dollars. *Paleobiology*, 5, 191–221.
https://doi.org/10.1017/S0094837300006527

Sheets, H.D. (2001) Integrated Morphometrics Package IMP: CoordGen8-Coordinate Generation Utility & PCAGen8-Principal Components Generation Utility: sheets@canisius.edu, Dept. of Physics, Canisius College, Main St. Buffalo, NY 14208, 716-888-2587.

Sievers, D. & Nebelsick, J.H. (2014) The petalodium of clypeasteroid sand dollars: A geometric morphometric description of

shape and comparison of fossil and living species [abstract]. *The Paleontological Society Special Publications*, 13, pp. 49–50.
https://doi.org/10.1017/S2475262200011059

Webster, M. & Sheets, H. (2010) A Practical Introduction to Landmark-based Geometric Morphometrics. *In*: Alroy, J. & Hunt, G. (Eds.), *Quantitative Methods in Paleobiology, Paleontological Society Short Course, October 30th, 2010,* 16. The Paleontological Society Papers, pp. 163–188.
https://doi.org/10.1017/S1089332600001868

Zachos, L.M. (2015) Holistic morphometric analysis of growth of the sand dollar *Echinarachnius parma* (Echinodermata:Echinoidea:Clypeasteroida). *Zootaxa,* 4052 (2), 151–179.
https://doi.org/10.11646/zootaxa.4052.2.1

Zelditch, M.L. (2005) Developmental regulation of variation. *In*: Hallgrimsson, B. & Hall, B.K. (Eds.), *Variation: a Central Concept in Biology*. Elsevier Academic Press, New York, pp. 249–276.
https://doi.org/10.1016/B978-012088777-4/50014-4

Zelditch, M.L., Swiderski, D.L., Sheets, H.D. & Fink, W.L. (2004) *Geometric Morphometrics for Biologists*. Elsevier Academic Press, New York, 443 pp.

Zelditch, M.L., Swiderski, D.L. & Sheets, H.D. (2012) *Geometric Morphometrics for Biologists: A Primer*. Second Edition. Elsevier Academic Press, San Diego, 478 pp.